nuclear fusion
IAEA

PAPER • OPEN ACCESS

High gas throughput SOLPS-ITER simulations extending the ITER database to strong detachment

To cite this article: J.D. Lore *et al* 2022 *Nucl. Fusion* **62** 106017

View the article online for updates and enhancements.

You may also like

- Assessment of ITER divertor performance during early operation phases
Jae-Sun Park, Xavier Bonnin and Richard Pitts
- Characterisation of highly radiating neon seeded plasmas in JET-ILW
S. Glöggler, M. Wischmeier, E. Fable et al.
- The role of plasma-molecule interactions on power and particle balance during detachment on the TCV tokamak
K. Verhaegh, B. Lipschultz, J.R. Harrison et al.

This content was downloaded from IP address 60.182.149.182 on 21/10/2023 at 21:28

OPEN ACCESS
IOP Publishing | International Atomic Energy Agency Nuclear Fusion
Nucl. Fusion **62** (2022) 106017 (10pp) https://doi.org/10.1088/1741-4326/ac8a5f

High gas throughput SOLPS-ITER simulations extending the ITER database to strong detachment

J.D. Lore[1,*], X. Bonnin[2], J.-S. Park[1], R.A. Pitts[2] and P.C. Stangeby[3]

[1] Oak Ridge National Laboratory, Oak Ridge, TN 37831, United States of America
[2] ITER Organization, Route de Vinon-sur-Verdon, CS 90 046, 13067 St Paul Lez Durance Cedex, France
[3] University of Toronto Institute for Aerospace Studies, Toronto, Canada

E-mail: lorejd@ornl.gov

Received 27 June 2022, revised 4 August 2022
Accepted for publication 17 August 2022
Published 7 September 2022

Abstract

SOLPS-ITER simulations performed for $Q_{DT} = 10$, $P_{SOL} = 100$ MW burning plasmas on ITER extend the existing database to high values of separatrix averaged neon impurity concentration ($\langle c_{Ne} \rangle \approx 6\%$) and divertor neutral pressure ($\langle p_{div} \rangle > 25$ Pa) in order to determine the heat flux mitigation capability of these scenarios and whether strongly detached states are accessible. In the existing database of ITER simulations, the level of detachment was limited to cases where the integral ion flux to the outer target was greater than 80% of the value at rollover, with the impurity radiation localized near the target. With the possibility of narrow heat flux channels and increased deposited power due to tile shaping, it is important to explore operation at a higher degree of detachment. Two series of simulations were explored to extend the database of SOLPS simulations. By increasing the deuterium and neon puff rates proportionally, the peak divertor energy flux ($q_{\perp,max}$) is decreased from 5 to 3 MW m^{-2} while $\langle p_{div} \rangle$ increased from 11 to 27 Pa. By increasing only the neon puff, $q_{\perp,max}$ can be reduced to <1MW m^{-2} while $\langle p_{div} \rangle$ is maintained at $\sim$11 Pa. As the neon puff level is increased, the position of the impurity radiation peak is shifted towards the X-point. At the highest neon puff levels with steady-state solutions, the electron temperature is reduced below 1 eV across 50 cm of each divertor target. The new cases extend previously observed tight relationships in power and momentum loss factors to low electron temperature improving their utility for highly detached regimes.

Keywords: SOLPS-ITER, ITER, divertor, detachment

(Some figures may appear in colour only in the online journal)

* Author to whom any correspondence should be addressed.

Original content from this work may be used under the terms of the Creative Commons Attribution 4.0 licence. Any further distribution of this work must maintain attribution to the author(s) and the title of the work, journal citation and DOI.

 © 2022 The Author(s). Published by IOP Publishing Ltd

1. Introduction[4]

The physics basis of the ITER divertor is informed by a database of steady-state simulations performed using the SOLPS code package [1–4]. This database spans a range of planned ITER operational scenarios, which determine inputs to the code such as input power into the scrape off layer (SOL) P_{SOL}, magnetic topology, and plasma-facing component materials. Given a set of these inputs and parameters related to the physics model (e.g., cross-field diffusivities, plasma-surface interactions, and activation of terms in the transport equations), SOLPS is used to predict the state of the boundary plasma and neutral particle distribution, as well as the fluxes to the plasma-facing components. The simulation database can be used to find operational windows of actuator inputs that result in acceptable performance. In particular, the fuel ion and impurity puff levels can be used to control the divertor fluxes and sputtering to reduce them below engineering limits [5]. At the same time, the upstream conditions act as boundary conditions for integrated simulations of the coupled core, pedestal, and boundary regions to find self-consistent solutions with acceptable performance to achieve ITER goals.

A significant part of the ITER simulation database has been performed for high-performance $Q_{\mathrm{DT}} = 10$ burning plasmas, with $P_{\mathrm{SOL}} = 100$ MW. The baseline transport assumptions, with cross-field diffusivities of $D_{\perp} = 0.3$, $\chi_{\perp} = 1.0$ m^2 s^{-1}, correspond to a outboard midplane (OMP) heat flux width of $\lambda_{\mathrm{q}} = 3.4$ mm [3]. The peak divertor energy flux and other key quantities have been shown to have tight correlations with scaling variables that enable effective sorting of the database. These are the impurity concentration $\langle c_Z \rangle = \sum n_Z/n_{\mathrm{e}}$ (where the sum is over the charge states of species Z) averaged along the main plasma separatrix, and a characteristic neutral pressure averaged over a volume in the private flux region [3]. The scaling variables have the advantage of directly relating divertor conditions to plasma parameters, instead of a specific actuator level, which has often been challenging to quantitatively validate against experimental conditions (typically as a mismatch between puff levels and measured neutral pressures) [6–8]. On the other hand, the actuator gas puff levels are the control parameters and correlated with the scaling variables.

The existing simulation database as presented in [3] spans a range of impurity concentrations and divertor neutral pressures of approximately $\langle c_{\mathrm{Ne}} \rangle < 2\%$, and $1 < \langle p_{\mathrm{div}} \rangle < 16$ Pa. The upper limits were selected to keep the outer divertor in a partially detached state, defined as the level where the integral ion flux to the outer target reaches 80% of the maximum level. Above this level the core radiation may increase, leading to instabilities, and neutrals may escape to the main chamber as the region of low temperature near the divertor surface increases. From a numerical perspective, the already significant computational time required to converge the code for large devices such as ITER (up to one month of wall clock time) increases under the low temperature, high density conditions of detached solutions. The computational cost has been eased by recent advances to the code which provide access to MPI and OpenMP parallelization, numerical strategies which greatly reduce the particle balance convergence time [9], and generally improved its stability and convergence properties. With the possibility of narrow heat flux channels in ITER, it is important to explore the flux mitigation capacity and neutral compression of strongly detached scenarios. Scaling relationships developed from empirical [10, 11] and theoretical models [12] result in predicted heat fluxes below 1 mm for ITER, however turbulent transport simulations [13, 14] have yielded larger values.

This paper presents new simulations which extend the database to $\langle c_{\mathrm{Ne}} \rangle = 6\%$, and $\langle p_{\mathrm{div}} \rangle = 30$ Pa to determine the heat flux mitigation capability of these scenarios and access to strongly detached states in ITER. The new simulations were performed using the most recent iteration of the code, SOLPS-ITER [15]. Two sets of new simulations are performed, one where the neon (Ne) and deuterium gas puff magnitudes are increased proportionally from a baseline level (maintaining approximately constant $\langle c_{\mathrm{Ne}} \rangle$) to achieve high $\langle p_{\mathrm{div}} \rangle$, and one where only the Ne puff level is increased to achieve high $\langle c_{\mathrm{Ne}} \rangle$. It is found that the high $\langle p_{\mathrm{div}} \rangle$ series approximately maintains previously observed trends in the reduction in the peak energy flux to the divertor, with only a modest increase in the level of detachment. The high $\langle c_{\mathrm{Ne}} \rangle$ series, on the other hand, results in the first observation of a strongly detached outer divertor in ITER ($T_{\mathrm{e}} < 1$ eV across 50 cm of both divertor targets) with the radiated power peak located upstream near the X-point. The effect of the increased puff levels on the downstream and upstream profiles, radiation patterns, and in terms of a reduced model for divertor detachment [16] are discussed. The SOLPS-ITER simulations indicate potential detached operational scenarios, assessed only from the boundary plasma perspective. Future simulations will consider integrated model solutions.

2. SOLPS-ITER simulation setup

The simulations are performed using the Release 3.0.8 version (commit acbdc5e5) of the SOLPS-ITER code, which solves a set of coupled continuity equations for particles, parallel momentum, energy, and current using a finite volume method. The magnetic equilibrium, initial plasma state, and code setup are taken from IMAS case number 123013, corresponding to full power operation with Ne impurity seeding. This baseline scenario has an input power of 100 MW, and deuterium and Ne gas puff values of 1.95×10^{23} and 2×10^{20} atoms s^{-1} delivered from the upper port entrance. A core ion flux of 1×10^{22} and 1×10^{20} particles per second is prescribed for fully stripped deuterium and helium,

[4] This manuscript has been authored in part by UT-Battelle, LLC, under contract DE-AC05-00OR22725 with the US Department of Energy (DOE). The publisher acknowledges the US government license to provide public access under the DOE Public Access Plan (http://energy.gov/downloads/doe-public-access-plan).

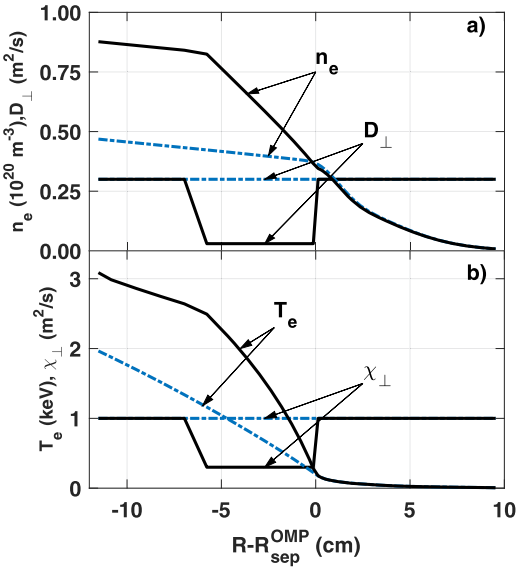

Figure 1. Profiles of (*a*) electron density and particle diffusivity and (*b*) electron temperature and thermal diffusivity at the OMP. Solid black lines indicate the case with an imposed core transport barrier, and the dashed blue lines the case without.

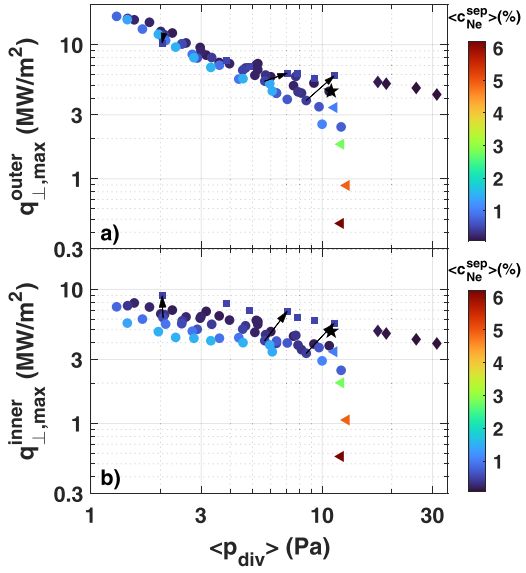

Figure 2. Maximum energy flux at the (*a*) outer and (*b*) inner divertor target as a function of the average neutral pressure in the divertor region. Circles are from the original SOLPS 4.3 data set, squares (connected by arrows) indicate the effect of updating the model to SOLPS-ITER, star is the initial case used to increase the D_2 and Ne puffs proportionally (diamonds) and only the Ne puff (triangles). Symbol color indicates the separatrix averaged Ne concentration.

respectively. A zero particle flux core boundary condition is used for all other ion species. Fluid plasma models are used for each charge state of deuterium, helium, and neon ions, with kinetic neutral treatment of atomic and molecular species. The setup of the kinetic neutral transport code EIRENE [17] uses the reaction model described in reference [18] which includes neutral–neutral elastic collisions between all of the present atomic and nuclear species.

A difference in this simulation setup, as compared to the majority of the cases presented in reference [3], is that the cross-field transport coefficients have a radial profile chosen to create a 'pedestal-like' pressure gradient in the core. The SOL diffusivity values are unchanged from those corresponding to heat flux width of 3.4 mm. Over a 6 cm region just inside the separatrix in the core region, the cross-field particle and thermal diffusivities were reduced. The same particle diffusivity values are used for all ion species, following the main database setup. Figure 1 shows the 'standard' diffusivities and the profiles used here, as well as the resulting electron density and temperature profiles at the OMP. This profile was selected to mimic an 'H-mode-like' pressure pedestal, as a first step towards integrated boundary-pedestal-core simulations, and to capture the reduced neutral and impurity ionization mean-free-paths that would be present in the ITER core.

Cross-field drifts are not activated in the simulations presented here. Transport barrier and drift effects have previously been included in SOLPS-ITER simulations of ITER [19], with the drifts shown to increase asymmetry in the inner and outer $q_{\perp,\mathrm{max}}$. While the results did not extend to the high levels of $\langle c_{\mathrm{Ne}} \rangle$ and $\langle p_{\mathrm{div}} \rangle$ described here, the effect was observed to be reduced as the level of detachment increases, e.g., at high $\langle p_{\mathrm{div}} \rangle$ [19]. A comparison to cases with constant transport coefficients has not yet been performed due to the significant computational cost of performing new simulations, and a detailed comparison of the effect on the neutral and impurity distribution is left for future work.

3. Results

3.1. Extension of the primary database

The peak heat fluxes to the inner and outer divertor from the initial dataset are shown in figure 2, as circular symbols plotted against $\langle p_{\mathrm{div}} \rangle$. The color of each symbol indicates the Ne impurity concentration $\langle c_{\mathrm{Ne}} \rangle$. The maximum target heat fluxes in figure 2 include contributions from the plasma (including surface recombination), neutral particles, and radiation (using a cylindrical approximation), assuming an axisymmetric divertor.

Two new series of simulations are added to the database to assess means of reducing the peak divertor fluxes, and to explore the limits of detachment without excessive core radiation. The initial (baseline) case is shown in figure 2 as a black star. In terms of the broader database, the baseline is already at the high end in terms of divertor neutral pressure, with $\langle p_{\mathrm{div}} \rangle \approx 11$ Pa, and a $\langle c_{\mathrm{Ne}} \rangle \approx 0.6\%$. Diamond symbols in figure 2 show results from a series of simulations where the D_2 and Ne gas puff magnitudes are increased from the baseline case (by factors of 1.5 to 3) while maintaining a constant ratio of the puff levels. Triangle symbols indicate a series of simulations where only the Ne puff level was increased by factors (up to 40 times the baseline level), while keeping the D_2 puff constant.

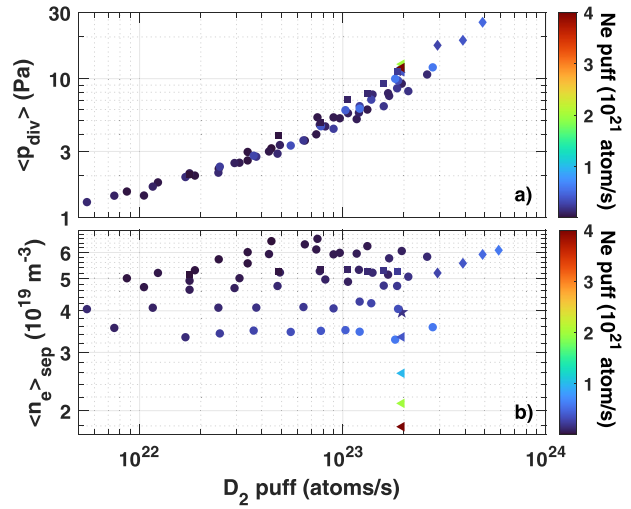

Figure 3. (*a*) Divertor neutral pressure and (*b*) separatrix electron density as a function of the D_2 puff magnitude. Symbol color indicates the Ne puff magnitude. Symbols have the same meaning as figure 2.

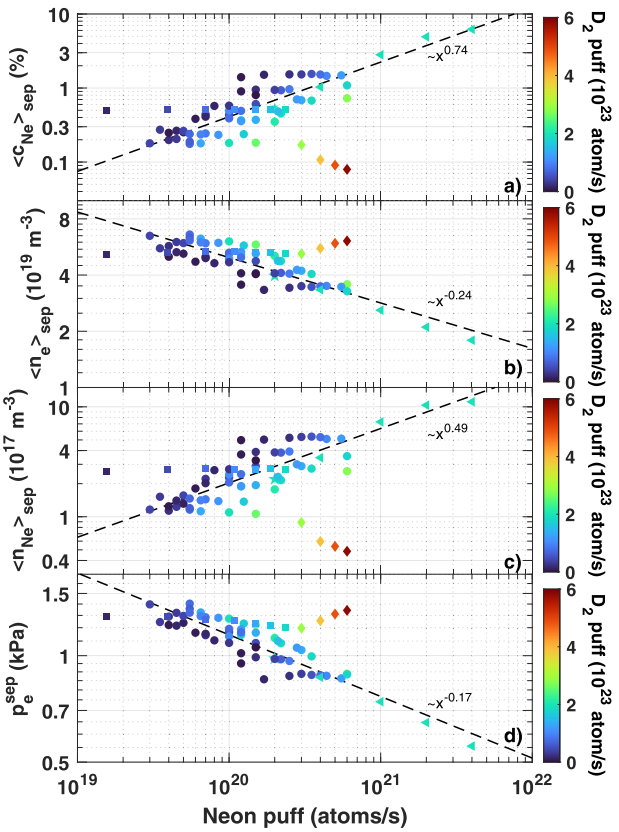

Figure 4. Separatrix averaged values of (*a*) Ne concentration, (*b*) electron density, (*c*) Ne density, and (*d*) electron static pressure as a function of the Ne puff magnitude. Symbol color indicates the D_2 puff magnitude. Symbols have the same meaning as figure 2. Lines indicate best log-space linear fits, excluding the highest D_2 puff series (4 diamond symbols).

All of the new additions to the database are using SOLPS-ITER, while original dataset was generated using SOLPS 4.3. Case 123013, with the 'H-mode like' profiles, does not have a corresponding database entry using the SOLPS 4.3 model. To assess the effect of differences in the physics model and numerical implementation between the code versions, three pairs of cases with the same actuator input levels run with SOLPS 4.3 and SOLPS-ITER are shown in figure 2. The SOLPS-ITER cases are plotted as square symbols, connected to the corresponding SOLPS 4.3 cases by an arrow. The primary effect is an increase in the peak divertor flux and in the divertor neutral pressure. The impact is larger on the inner divertor. For the purposes of this work, it is assumed that the qualitative behaviour of the trends does not significantly change between the models despite this quantitative change. Details of the changes to the code physics and numerical models can be found in [15, 20], and quantifying the effects is beyond the scope of this paper. However, a primary effect is thought to be the plasma-neutral interaction and excitation radiation models, e.g., switching from STRAHL [21] to ADAS [22]. The electron cooling rate of the Ne ion primary radiators (Ne^{3+}–Ne^{7+}) differs between ADAS and STRAHL up to a factor of 2 depending on the charge state and T_e. Accordingly, the SOLPS calculation result when ADAS is used for total radiated power is reduced by about 10%–20% compared to when STRAHL is used, meaning that SOLPS-4.3 databases using STRAHL show an increased heat flux reduction.

The high D_2 gas puff series shows a continual reduction in the peak energy flux density with increasing $\langle p_{div} \rangle$. Accounting for the differences in the code versions and setup, the trend is approximately exponential at constant $\langle c_{Ne} \rangle$ on the inner divertor, but indicates signs of flattening out on the outer divertor at high $\langle p_{div} \rangle$. Increasing $\langle p_{div} \rangle$ to ≈30 Pa results in a peak energy flux of ≈4 MW m^{-2} on each divertor.

The highest pressure case corresponds to a D_2 fuelling rate of 5.85×10^{23} atoms s^{-1}, which is within the capabilities of the ITER gas system. The total throughput (core fuelling plus gas puff) which must be removed by the pumping system in steady-state operation, however, exceeds the stationary capacity of 1×10^{23} atoms s^{-1} for the ITER divertor cryopumps.

The high $\langle c_{Ne} \rangle$ series shows a significant decrease in the energy flux density to both the inner and outer divertor, with the peak level dropping below 1 MW m^{-2} on each. While the reduction is significant, it should be noted that $q_{\perp,max}$ remains inversely proportional to the Ne puff level (e.g., a factor of 2 increase in the Ne puff was required to reduce $q^{outer}_{\perp,max}$ from 0.9 MW m^{-2} to 0.4 MW m^{-2}), and no sharp discontinuity is observed. This is promising from the perspective of detachment control, however analysis of the simulation dynamics must be performed. On the other hand, the highest Ne gas puff shown is the last level for which stable code results were found. Doubling the gas puff from this state results in a simulation where the divertor T_e continues to drop while the core radiation increases, with no stable solution. This may indicate a threshold level where strong nonlinearities (e.g., in the rate coefficients at low T_e) lead to radiative collapse of the core plasma. The threshold level is also expected to be affected by cross-field drifts, which generally cause asymmetry in the

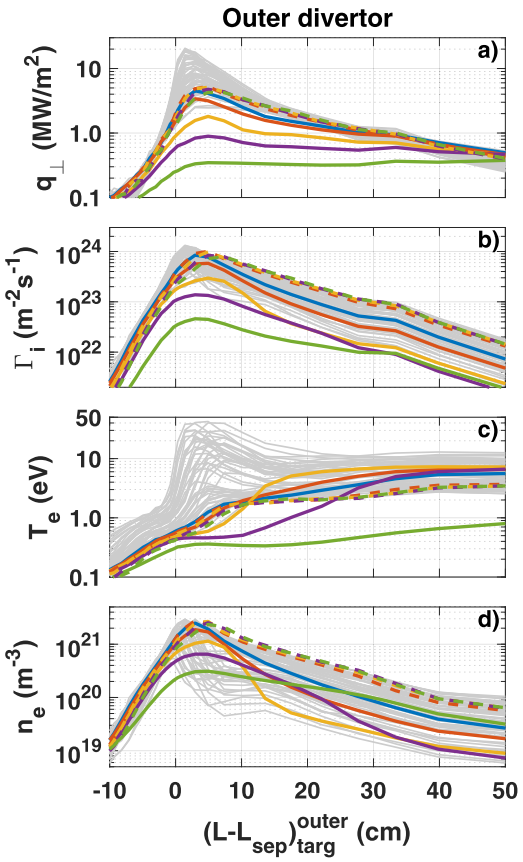

Figure 5. Outer divertor profiles of (*a*) deposited energy flux, (*b*) deposited ion flux, (*c*) electron temperature, and (*d*) electron density. Gray lines are from the SOLPS 4.3 data set, with colored lines showing the profiles from the high Ne puff series (solid) and high D_2 puff series (dashed).

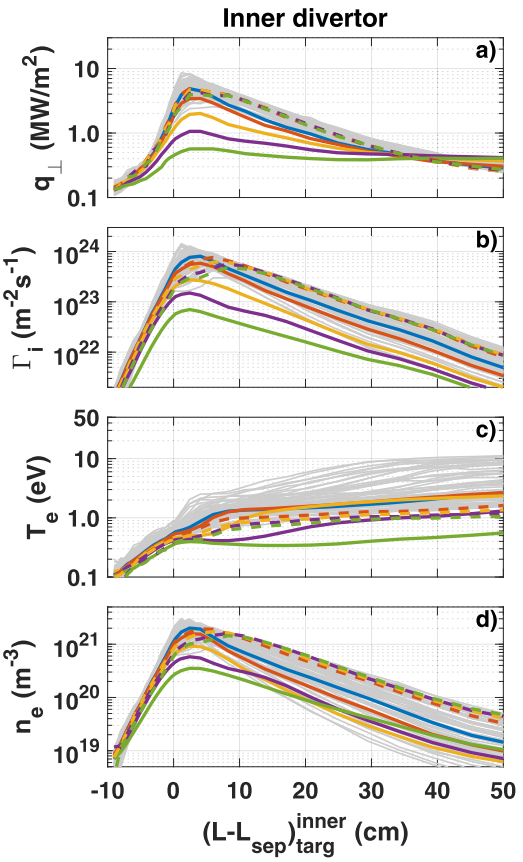

Figure 6. Inner divertor profiles of (*a*) deposited energy flux, (*b*) deposited ion flux, (*c*) electron temperature, and (*d*) electron density. Gray lines are from the SOLPS 4.3 data set, with colored lines showing the profiles from the high Ne puff series (solid) and high D_2 puff series (dashed).

inner and outer divertor fluxes and may lead to rapid transitions in the divertor state [23, 24], although at higher levels of detachment (high $\langle p_{\mathrm{div}} \rangle$) the effect of drifts on the divertor fluxes is reduced [19]. The impact of the validity of the plasma-neutral reaction rate coefficients at low T_e values, including treatment of extrapolation, can also affect the convergence behaviour and steady-state solutions [25, 26]. Radiation transport (not included here), has also been shown to affect stability for detached plasma simulations [18]. Investigation of these effects is computationally expensive, however, and outside the scope of this work.

As discussed in reference [3], the actual ITER divertor has shaped tiles that result in a larger angle of incidence. Accounting for this shaping increases the angle of incidence by approximately 1.5 degrees, which affects only the plasma component of the total energy flux density. Accounting for this effect increases the plasma component by a factor of ≈1.5 near the strike point on the outer divertor, increasing to a factor of ≈3.5 50 cm away from the strike point. On the inner divertor these factors are ≈1.5 and ≈2.5, respectively. As the fraction of the total flux carried by the plasma reduces as the level of detachment increases (increasing $\langle c_{\mathrm{Ne}} \rangle$ and $\langle p_{\mathrm{div}} \rangle$), this larger angle of incidence has a stronger effect for the points on the left side of figure 2 and results in a steeper slope in the trends. This analysis only accounts for the geometric effect on the deposited fluxes, and not for the correspondingly increased flux of recycled neutrals, which would impact the plasma solution and require a more complex treatment to reach a self-consistent solution.

3.2. Relationship between scaling variables and gas puff inputs

When interpreting predictive SOLPS simulations, arguments can be made for different selections of variables to be compared to the expected experimental conditions. Interpretive analysis and experimental validation has shown that simultaneously matching upstream and downstream plasma conditions and neutral pressures using the experimental actuator inputs is extremely challenging. The variables $\langle c_{\mathrm{Ne}} \rangle$ and $\langle p_{\mathrm{div}} \rangle$ have been shown to be effective in sorting the simulation outputs of interest, and can (in principle) be measured. During operation, the downstream solution can then be 'tuned' to the appropriate actuator levels and the relationship between the inputs used to guide control strategies. That is, as long the direction of the change in the desired state with respect to the actuator level is correct, a systematic offset still allows for successful control. On the other hand, the actuator levels are the inputs for experimental operation, and the relationship

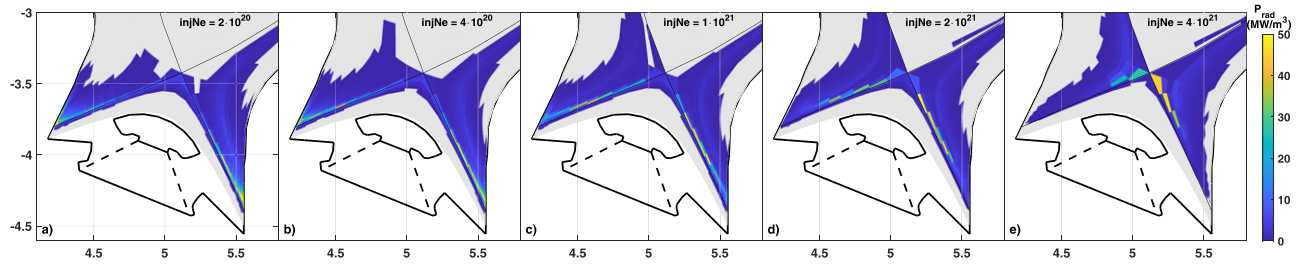

Figure 7. Radiated power density for the high Ne puff series, showing the peak density moving from the divertor region to the X-point as the puff magnitude increases.

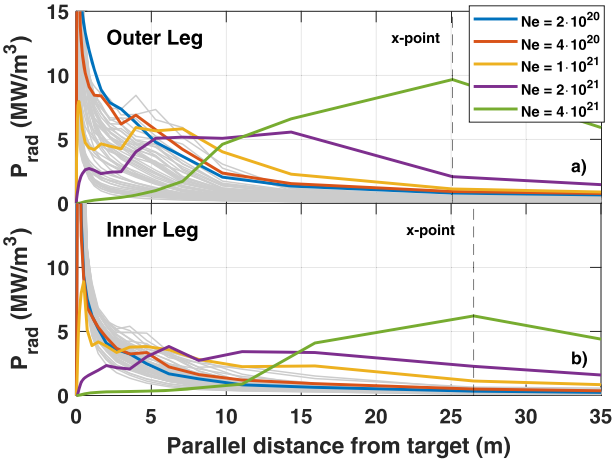

Figure 8. Radiated power density averaged across the SOL in the (*a*) outer and (*b*) inner divertor region plotted as parallel distance along the separatrix leg from the target. Gray lines are from the SOLPS 4.3 data set, with colored lines showing the profiles from the high Ne puff series.

between the actuators and effective sorting variables should be explored.

The relationships between the variables $\langle p_{\mathrm{div}} \rangle$ and $\langle c_{\mathrm{Ne}} \rangle$ and the actuator inputs are shown in figures 3(*a*) and 4(*a*). The divertor pressure is well correlated with the D_2 gas puff, while the Ne concentration is a function of both gas puff inputs. This complex relationship can be explored by examining the effect of each gas puff on the separatrix electron density. As shown in figure 3(*b*), $\langle n_{\mathrm{e}} \rangle$ only increases slowly (or not at all) with the D_2 puff strength at constant $\langle c_{\mathrm{Ne}} \rangle$, indicating that the injected D_2 partially acts to increase the divertor pressure without significantly increasing the core particle content. Increasing the Ne gas puff strength, on the other hand, causes a strong reduction in $\langle n_{\mathrm{e}} \rangle$ (figure 4(*b*)) along with an increase in the separatrix Ne density (figure 4(*c*)). The former effect has been attributed to the increased energy loss from Ne radiation reducing the available energy for deuterium ionization causing a reduction in the ion source [3], but is also affected by the reduced recycling ion flux as the divertor detaches.

The net effect of the trends in $\langle n_{\mathrm{e}} \rangle$ and $\langle c_{\mathrm{Ne}} \rangle$ yield the scaling in $\langle c_{\mathrm{Ne}} \rangle$ with Ne puff shown in figure 4(*a*). The upstream static electron pressure shows a reduction with increasing Ne puff, however the high $\langle c_{\mathrm{Ne}} \rangle$ still show an increased momentum and power dissipation from upstream to the divertor as discussed in section 3.5. The decrease in $\langle n_{\mathrm{e}} \rangle$ and $p_{\mathrm{e}}^{\mathrm{sep}}$ can be counteracted by increasing the D_2 puff, as indicated by the series of diamond symbols in figure 4, however these correspond to the low $\langle c_{\mathrm{Ne}} \rangle$ cases with modest reduction in the divertor flux shown in figure 2. These results again highlight the need for integrated core-pedestal-boundary simulations, as the operational scenarios must simultaneously satisfy the divertor flux limits, upstream density, core impurity content, and gas throughput requirements of ITER.

3.3. Effect on divertor profiles

The outer and inner divertor profiles of (*a*) deposited energy flux, (*b*) deposited ion particle flux, (*c*) electron temperature, and (*d*) electron density on the outer and inner divertor are shown in figures 5 and 6. The grey lines are profiles from the original database. The solid blue line is the 'baseline' case, with the other solid lines the high Ne puff series, and the dashed line the series with both puffs scaled proportionally. As noted above, the baseline case is already in a partially-detached condition, with gas puff levels (or $\langle p_{\mathrm{div}} \rangle$ and $\langle c_{\mathrm{Ne}} \rangle$) resulting in peak divertor fluxes and electron temperatures towards the lower range of the database. The series with both puffs scaled proportionally result in only a modest increase in the detachment level, and even then only near the strike point and primarily on the inner divertor. The high Ne puff cases, on the other hand, result in significantly reduced $q_{\perp}$, Γ_{i}, and T_{e}, with the reduction increasing in magnitude and moving radially outward with increasing Ne puff. At the highest Ne puff, T_{e} is reduced below 1 eV and $q_{\perp,\mathrm{max}}$ below 1 MW m^{-2} across 50 cm of each divertor target, and the integrated target ion flux and peak n_{e} show a clear rollover. This result is the first observation of strongly suppressed electron temperature across the divertor plate for an ITER simulation.

To estimate if neutral particles will be well confined to the divertor region, the ionization mean free path of the Franck Condon neutral atoms (≈3 eV) can be compared to the shortest characteristic path length for them to escape. This value is ≈0.5–1.0 m in the ITER divertor, either to travel from the strike point to the X-point (or to move from the strike point to the far-SOL along the divertor plate in the poloidal plane). In the baseline case, for the original database simulations, and for the high $\langle p_{\mathrm{div}} \rangle$ cases, the ratio of these quantities is small

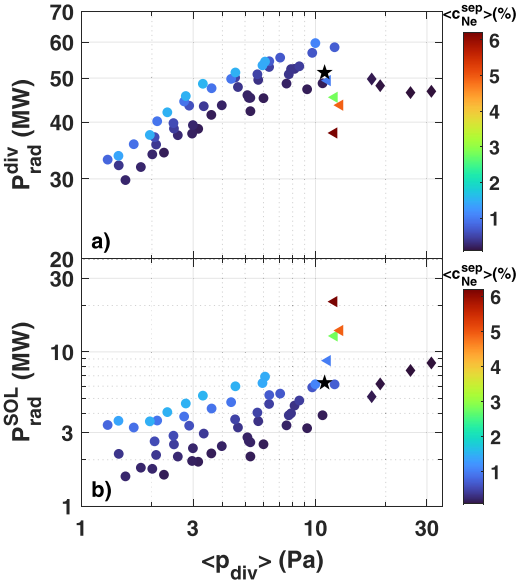

Figure 9. Radiated power in the (*a*) inner and outer divertor regions (below the X-point) and (*b*) SOL region (SOL above the X-point). Symbols have the same meaning as figure 2.

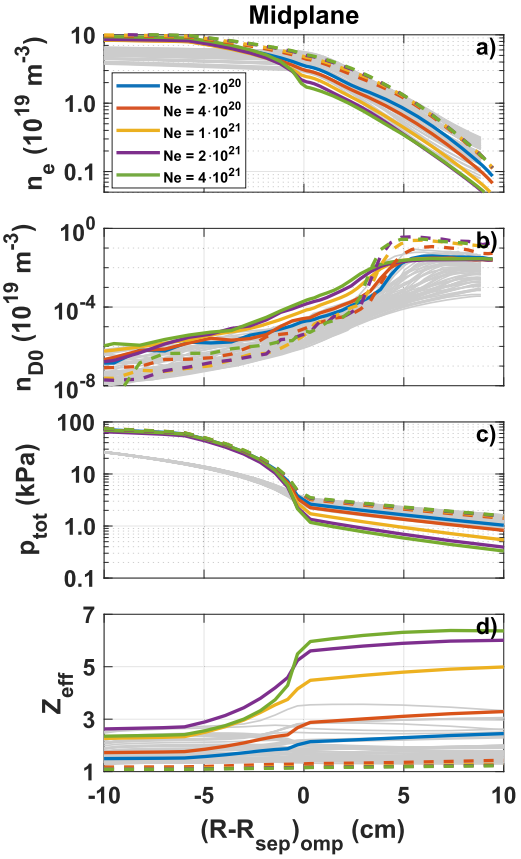

Figure 10. OMP profiles of (*a*) electron density, (*b*) electron temperature, (*c*) total pressure, and (*d*) Z_{eff}. Gray lines are from the SOLPS 4.3 data set, with colored lines showing the profiles from the high Ne puff series (solid) and high D_2 puff series (dashed).

for at least some portion of the neutral trajectory (near the strike point) and the neutral density in the near-SOL and core region is negligible. At the high Ne concentrations, on the other hand, the ionization mean free path exceeds 1 m across the inner divertor and for a narrow region on the outer divertor, allowing neutral particles to escape. At the highest $\langle c_{\mathrm{Ne}} \rangle$ with stable code results, neutral deuterium and Ne atoms begin to penetrate across the separatrix near the midplane and at the top of the device. The strong nonlinearities in the impurity cooling and ionization curves at low T_{e} and the reduced SOL density can lead to an unstable scenario where the impurities and neutrals penetrate further into the core, likely resulting in the inability to converge the code at higher gas puff levels. The exact values at which this occurs will depend on the physical dimensions of the device, the assumptions made for the H-mode pedestal parameters, and the core boundary conditions. It may be expected that at some level, increasing the impurity puff will cause $\langle p_{\mathrm{div}} \rangle$ to drop as the neutral 'plugging' (short ionization mean free path) by the plasma is reduced, which could result in the triangle series of points in figure 2 to move to the left. So far this trend has not been clearly observed. The core neutral density profile is discussed further in section 3.5.

3.4. Effect on radiated power distribution

The reduced target fluxes correspond to a shift in the peak radiated power density away from the divertor surface towards the X-point. The 2D distributions of P_{rad} are shown in figure 7 for the high Ne puff series. Figure 8 shows P_{rad} averaged across the SOL flux tubes as a function of parallel distance from the target, with the values from the original database shown in grey. For an injection rate below 1×10^{21} atoms s^{-1} the radiated power is localized near the divertor surface. In the range of $1\text{–}2 \times 10^{21}$ atoms s^{-1}, P_{rad} is peaked towards the middle of the separatrix leg in the poloidal plane, and at 4×10^{21} atoms s^{-1} it is peaked near the X-point. The total radiated power in the upper SOL (defined as the flux tube from inner X-point to outer X-point) is less than 7 MW in the original database ($\approx$7% of P_{SOL}), and increases to 21 MW at the highest Ne puff level ($\approx$29% of P_{SOL}). The core radiated power density is low in the X-point region across the scan, however high charge state Ne crosses the separatrix near the midplane and at the top of the device, with the total core radiation reaching 8 MW compared to a peak value of 4 MW in the original database, ($\approx$4% and $\approx$11% of P_{SOL}, respectively).

The integrated radiated power in the divertor and SOL regions is shown in figure 9. Here the regions correspond to the SOLPS-ITER volumes, where the divertor regions extend from the poloidal position of the X-point to the divertor target, and the SOL region from the inner to outer X-point. Corresponding to the shift of the radiation upwards away from the divertor surface, the divertor radiation drops with increasing Ne puff, while the SOL radiation increases.

3.5. Upstream profiles and loss factors

Profiles of (*a*) n_{e}, (*b*) n_{D0}, (*c*) total pressure $p_{\mathrm{tot}} = n_{\mathrm{e}}T_{\mathrm{e}} + \Sigma n_{\mathrm{a}}(T_{\mathrm{i}} + m_{\mathrm{a}}v^2_{\mathrm{a}\|})$, and (*d*) Z_{eff} at the OMP are shown in figure 10, using the same color scheme as figure 5. The

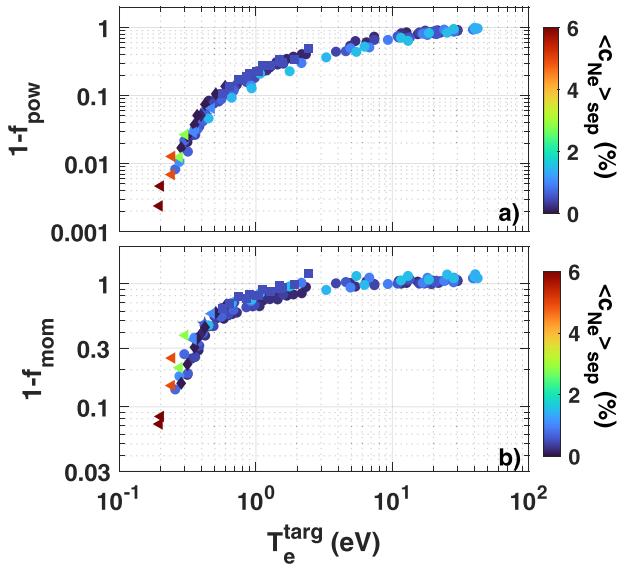

Figure 11. Loss factors for (*a*) power and (*b*) momentum in the third and fourth flux tube from the separatrix as a function of the electron temperature at the target. Symbol color indicates the separatrix averaged Ne concentration. Symbols have the same meaning as figure 2.

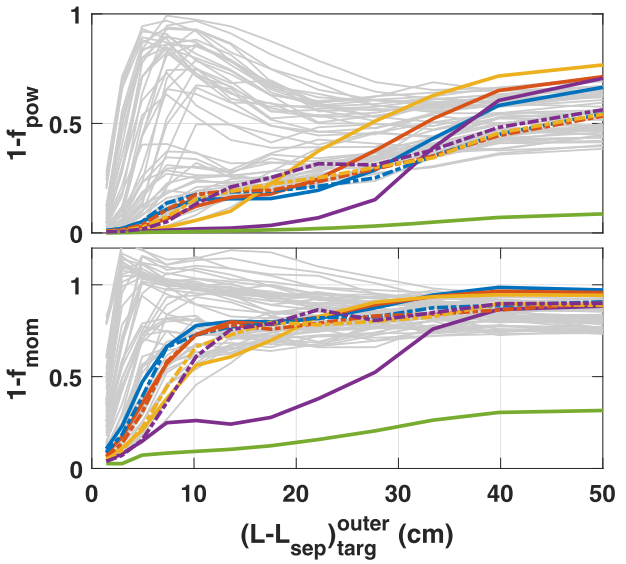

Figure 12. Radial profiles of loss factors for (*a*) power and (*b*) momentum mapped to the outer divertor.

reduction in n_e and p_{tot} at the separatrix and in the SOL with increasing $\langle c_{Ne} \rangle$ can be clearly seen. The neutral atom density is here defined as the average value (accounting for cell volumes) in each flux tube at the top of the device, the portion extending from the inboard to OMP. This definition ignores the X-point region, and shows the effect on the neutral density in the upper-SOL. As $\langle c_{Ne} \rangle$ increases, the neutral atoms penetrate further into the core due to both the increased ionization mean free path in the lower divertor region as well as the lower SOL density. The high $\langle p_{div} \rangle$ series (dashed lines) shows an increase in the SOL neutral density at the top of the device, the region where the gas puffs are located in these simulations. This increase in the SOL neutral density is physically separated from the high neutral pressure in the subdivertor, however the increased total particle content leads to the increased recycling flux that drives the higher neutral pressure at the pumping surfaces (and $\langle p_{div} \rangle$) required to maintain particle balance.

The Z_{eff} increases to ≈6 at the highest Ne puff. At this level the core plasma may not be compatible with ITER operational scenarios, and it is unlikely that such a low separatrix electron density would be acceptable. Future simulations will explore self-consistent solutions, via coupling of boundary conditions with core impurity transport models.

The existing and extended database has been used to calculate factors that describe the momentum and power loss from upstream to the divertor, extending the range of applicability of the reduced models. These factors contain the integrated pressure drop and momentum loss (along the flux tube of interest), which can be used to develop simplified models for predicting divertor parameters [16]. The loss factors are defined as the ratio of the target to upstream values of the total pressure (for $1 - f_{mom}$), and the product of major radius and parallel heat flux density (for $1 - f_{cool}$). Here the upstream profiles are taken from the poloidal index of the X-point, which is approximately the poloidal position of the peak parallel heat flux density. Figure 11 shows the outer divertor values in the third and fourth flux tubes from the separatrix, corresponding to flux tubes where the peak divertor fluxes typically occur (3–5 cm from the separatrix along the outer divertor). It is found that the factors continue to be relatively tight functions of the target electron temperature, even under the high impurity concentration and divertor pressure conditions.

This simple relationship has the same caveat as noted in reference [16], that the range of input parameters such as input power and radial transport coefficients is very limited for the ITER database used here. The new cases extend the trends to the lowest T_e values and strongest dissipation values in this dataset for flux tubes 3 and 4. The radial profiles of the loss factors are shown in figure 12 for each flux tube in the SOL. As the Ne puff increases, the radial extent of the detachment region increases, with significant momentum and power loss. Note that the pressure drop persists despite the reduction in the upstream total pressure. At the highest Ne puff level, strong detachment is observed across the entire divertor target.

4. Conclusions

The two new series of SOLPS-ITER simulations, obtained by increasing the D_2 and Ne puff at a fixed ratio (approximately constant $\langle c_{Ne} \rangle$) and only increasing the Ne puff (approximately constant $\langle p_{div} \rangle$) have extended the existing database of SOLPS simulations of ITER. The high $\langle p_{div} \rangle$ cases approximately continue previously observed trends in reducing the peak divertor flux, accounting for difference in the input file setup and models between the code versions. Along this series of runs, the effect on the divertor parameters is relatively modest and localized near the separatrix, and strong detachment

is not observed. Although the subdivertor neutral pressure continues to increase strongly with increasing D_2 puff, the upstream n_e increases at a slower rate. The injected D_2 has the primary effect of increasing the divertor recycling ion source through the global particle balance, with no bifurcation in the recombination source or neutral pathways through increased ionization mean free path observed over the range scanned.

The high $\langle c_{Ne} \rangle$ cases show a path to strong detachment, albeit at significantly increased Ne puff levels, reduced upstream electron density, and increased upstream Z_{eff}. Despite the strong detachment, and the movement of the peak radiated power up the separatrix legs towards the X-point, no significant radiated power is observed in the core. A 20× increase in the Ne puff results in the core radiation increasing from 4 MW to 8 MW. The movement of the simulated radiation front is expected to be observable by the ITER bolometry system [27, 28], and the reduction in the divertor flux and T_e is inversely proportional to the Ne puff level without discontinuous behavior that is sometimes observed in experiment and simulation, e.g., the 'T_e cliff' seen in DIII-D [24, 29]. These observations are promising for potential control of the detachment level by gas input. However it must be noted that the plasma response times (from dynamic simulations), actuator and diagnostic latency, and inclusion of effects such as cross-field drifts, that may impact the trends must be addressed in evaluating control of these scenarios.

An additional simulation with the Ne puff level doubled again failed to converge, with the divertor temperature dropping and the radiated power increasing until the equation residuals reached a level where the run was halted. Future simulations can attempt to characterize the stability boundary, which may be very sharp due to the strong nonlinearities in rate coefficients that occur at low electron temperature.

The SOLPS-ITER simulations presented are an attempt to extend the ITER database, and only model the boundary plasma without consideration for other aspects of ITER operation. The strongly detached solutions may not be accessible for a variety of reasons. The ITER pumping system can handle 200 Pa m^3 s^{-1} in steady-state, although this may be exceeded for a short duration. The gas system is expected to be able to handle the D_2 and Ne puff rates scanned, however it has been observed in current devices that the absolute values of experimental gas puff levels do not necessarily correspond to the observed plasma solution or neutral pressure values measured at gauges [6–8]. Accounting for this discrepancy is part of a broader effort to validate SOLPS-ITER solutions, constrain ad-hoc inputs such as the cross-field transport coefficients (including those for impurity ions which will affect the concentration), and improve the physics model in the code. At the same time, qualitative trends are often in agreement with experimental observations, and finding boundary solutions that have acceptable, stable, conditions is useful for mapping out future operational regimes. Coupled core-pedestal-boundary simulations are absolutely required to find integrated solutions. The ad-hoc inclusion of a 'pedestal' transport barrier in the simulations presented here is a step in this direction, however the impact on the core impurity concentration (and effects such as temperature gradient force on the impurities) remains to be assessed.

Acknowledgments

Work supported, in part, by the US Department of Energy under Contract No. DE-AC05-00OR22725 with UT-Battelle LLC, and by the Office of Science, Office of Fusion Energy Sciences and Office of Advanced Scientific Computing Research through the Scientific Discovery through Advanced Computing (SciDAC) project on Plasma-Surface Interactions. The views and opinions expressed herein do not necessarily reflect those of the ITER Organization. The publisher acknowledges the US government license to provide public access under the DOE Public Access Plan (http://energy.gov/downloads/doe-public-access-plan). This research used resources of the Compute and Data Environment for Science (CADES) at the Oak Ridge National Laboratory, which is supported by the Office of Science of the U.S. Department of Energy under Contract No. DE-AC05-00OR22725.

ORCID iDs

J.D. Lore https://orcid.org/0000-0002-9192-465X
J.-S. Park https://orcid.org/0000-0003-0871-7527
R.A. Pitts https://orcid.org/0000-0001-9455-2698

References

[1] Kukushkin A.S., Pacher H.D., Kotov V., Pacher G.W. and Reiter D. 2011 *Fusion Eng. Des.* **86** 2865
[2] Pacher H.D., Kukushkin A.S., Pacher G.W., Kotov V., Pitts R.A. and Reiter D. 2015 *J. Nucl. Mater.* **463** 591
[3] Pitts R.A. *et al* 2019 *Nucl. Mater. Energy* **20** 100696
[4] Park J.-S., Bonnin X. and Pitts R. 2021 *Nucl. Fusion* **61** 016021
[5] Dux R., Loarte A., Angioni C., Coster D., Fable E. and Kallenbach A. 2017 *Nucl. Mater. Energy* **12** 28
[6] Varoutis S., Gleason-González C., Moulton D., Kruezi U., Groth M., Day C., Wiesen S. and Harting D. 2017 Simulation of neutral gas flow in the JET sub-divertor *Fusion Eng. Des.* **121** 13
[7] Wiesen S. *et al* 2018 On the role of finite grid extent in SOLPS-ITER edge plasma simulations for JET H-mode discharges with metallic wall *Nucl. Mater. Energy* **17** 174
[8] Reksoatmodjo R., Mordijck S., Hughes J.W., Lore J.D. and Bonnin X. 2021 The role of edge fueling in determining the pedestal density in high neutral opacity Alcator C-Mod experiments *Nucl. Mater. Energy* **27** 100971
[9] Kaveeva E., Rozhansky V., Senichenkov I., Veselova I., Voskoboynikov S., Sytova E., Bonnin X. and Coster D. 2018 *Nucl. Fusion* **58** 126018
[10] Eich T. *et al* 2013 *Nucl. Fusion* **53** 093031
[11] Brunner D., LaBombard B., Kuang A.Q. and Terry J.L. 2018 *Nucl. Fusion* **58** 094002
[12] Goldston R.J. 2012 *Nucl. Fusion* **52** 013009
[13] Chang C.S. *et al* 2017 *Nucl. Fusion* **57** 116023
[14] Xu X.Q., Li N.M., Li Z.Y., Chen B., Xia T.Y., Tang T.F., Zhu B. and Chan V.S. 2019 *Nucl. Fusion* **59** 126039
[15] Bonnin X., Dekeyser W., Pitts R., Coster D., Voskoboynikov S. and Wiesen S. 2016 Presentation of the new SOLPS-ITER

code package for tokamak plasma edge modelling *Plasma Fusion Res.* **11** 1403102
[16] Stangeby P.C. 2018 *Plasma Phys. Control. Fusion* **60** 044022
[17] Reiter D., Baelmans M. and Börner P. 2005 The EIRENE and B2-EIRENE codes *Fusion Sci. Technol.* **47** 172
[18] Kotov V., Reiter D. and Wiesen S. 2013 Self-consistent modeling of X-point MARFE and divertor detachment *J. Nucl. Mater.* **438** S449–52
[19] Kaveeva E. *et al* 2020 *Nucl. Fusion* **60** 046019
[20] Wiesen S. *et al* 2015 *J. Nucl. Mater.* **463** 480
[21] Behringer K. 1987 *Report JET-R(87)08* (Culham: JET Joint Undertaking)
[22] Summers H.P. *et al* 2007 ADAS: Atomic data, modelling and analysis for fusion *AIP Conf. Proc.* **901** 239
[23] Du H., Zheng G., Guo H., Jaervinen A.E., Duan X., Bonnin X., Eldon D. and Wang D. 2020 *Nucl. Fusion* **60** 046028
[24] Jaervinen A.E. *et al* 2018 *Phys. Rev. Lett.* **121** 075001
[25] Moscheni M. *et al* 2022 *Nucl. Fusion* **62** 056009
[26] Rivals N., Tamain P., Marandet Y., Boinin X., Bufferand H., Pitts R.A., Falchetto G., Yang H. and Ciraolo G. 2022 *Contrib. Plasma Phys.* **62** e202100182
[27] Meister H. *et al* 2019 *J. Inst.* **14** C10004
[28] Brank M. 2022 Assessment of the ITER divertor bolometer diagnostic performance, PSI-25 conference *Nucl. Mater. Energy* (in preparation)
[29] Eldon D. *et al* 2017 Controlling marginally detached divertor plasmas *Nucl. Fusion* **57** 066039